Calcium Wave Promotes Cell Extrusion

Yasuto Takeuchi,[1,10] Rika Narumi,[1,10] Ryutaro Akiyama,[2,10] Elisa Vitiello,[3] Takanobu Shirai,[1] Nobuyuki Tanimura,[1] Keisuke Kuromiya,[1] Susumu Ishikawa,[1] Mihoko Kajita,[1] Masazumi Tada,[4] Yukinari Haraoka,[5] Yuki Akieda,[5] Tohru Ishitani,[5] Yoichiro Fujioka,[6] Yusuke Ohba,[6] Sohei Yamada,[2,7] Yoichiroh Hosokawa,[7] Yusuke Toyama,[8,9] Takaaki Matsui,[2,*] and Yasuyuki Fujita,[1,11,*]

[1]Division of Molecular Oncology, Institute for Genetic Medicine, Hokkaido University Graduate School of Chemical Sciences and Engineering, 060-0815 Sapporo, Japan

[2]Gene Regulation Research, Division of Biological Science, Graduate School of Science and Technology, Nara Institute of Science and Technology, 630-0101 Ikoma, Japan

[3]Cancer Research UK Cambridge Institute, University of Cambridge, CB2 0RE Cambridge, UK

[4]Department of Cell and Developmental Biology, University College London, WC1E 6BT London, UK

[5]Department of Homeostatic Regulation, Division of Cellular and Molecular Biology, Research Institute for Microbial Diseases, Osaka University, 565-0871 Osaka, Japan

[6]Department of Cell Physiology, Faculty of Medicine and Graduate School of Medicine, Hokkaido University, 060-8638 Sapporo, Japan

[7]Bio-Process Engineering Laboratory, Division of Material Sciences, Graduate School of Science and Technology, Nara Institute of Science and Technology, 630-0101 Ikoma, Japan

[8]Mechanobiology Institute, National University of Singapore, 117411 Singapore

[9]Department of Biological Sciences, National University of Singapore, 117543 Singapore

[10]These authors contributed equally

[11]Lead Contact

*Correspondence: matsui@bs.naist.jp (T.M.), yasu@igm.hokudai.ac.jp (Ya.F.)

SUMMARY

When oncogenic transformation or apoptosis occurs within epithelia, the harmful or dead cells are apically extruded from tissues to maintain epithelial homeostasis. However, the underlying molecular mechanism still remains elusive. In this study, we first show using mammalian cultured epithelial cells and zebrafish embryos that prior to apical extrusion of RasV12-transformed cells, calcium wave occurs from the transformed cell and propagates across the surrounding cells. The calcium wave then triggers and facilitates the process of extrusion. IP_3 receptor, gap junction, and mechanosensitive calcium channel TRPC1 are involved in calcium wave. Calcium wave induces the polarized movement of the surrounding cells toward the extruding transformed cells. Furthermore, calcium wave facilitates apical extrusion, at least partly, by inducing actin rearrangement in the surrounding cells. Moreover, comparable calcium propagation also promotes apical extrusion of apoptotic cells. Thus, calcium wave is an evolutionarily conserved, general regulatory mechanism of cell extrusion.

KEYWORDS

Calcium wave; epithelial homeostasis; cell extrusion; RasV12-transformed; apoptosis; actin rearrangement; TRPC1; INF2

INTRODUCTION

In order to maintain harmonious and coordinated cellular society, epithelial tissues are equipped with several homeostatic mechanisms to actively eliminate harmful or suboptimal cells from epithelial layers. Among them, apical cell extrusion plays a vital role in eradication of transformed or apoptotic epithelial cells, especially in vertebrates. For instance, when oncogenic transformation such as Ras, Src, or ErbB2 occurs in single cells within epithelia at the initial stage of carcinogenesis, newly emerging transformed cells are often extruded into the apical lumen of an epithelial monolayer; the process of apical extrusion has been observed in cultured cells and zebrafish and mouse *in vivo* model systems [1-6]. When transformed cells alone are present, they stay in a monolayer, suggesting that the presence of surrounding normal cells induces apical extrusion of the transformed cells. In addition to transformed cells, apoptotic cells are also apically eliminated from epithelial monolayers [7]. Several lines of evidence suggest that cell-cell communication between the extruded and surrounding cells triggers the process of apical extrusion, however, the underlying molecular mechanisms are still largely unknown.

Calcium signaling plays a versatile role in cell-cell communication [8, 9]. In this study, we demonstrate that calcium wave occurs from the extruding cell and propagates across the surrounding cells, which triggers and facilitates the process of cell extrusion.

RESULTS

Calcium Wave Triggers and Facilitates Apical Extrusion of RasV12-Transformed Cells

To examine whether and how calcium signaling is involved in the intercellular communication between normal and transformed epithelial cells, we have established Madin-Darby canine kidney (MDCK) epithelial cells stably expressing GCaMP6S, a GFP-based intracellular calcium sensor (Figure S1A) [10, 11]. When Myc-RasV12 and mCherry were transiently co-expressed in a mosaic manner within a monolayer of MDCK-GCaMP6S cells, RasV12-expressing cells were apically extruded as observed within that of parental MDCK cells (Figure S1B) [1]. Time-lapse analyses revealed that before the apical extrusion started, the calcium level of RasV12 cells was acutely elevated, which then induced an explosive calcium propagation through the surrounding normal cells (Figures 1A, 1C, S1C, S1D, Videos S1). In most cases, this intercellular calcium propagation, hereafter called calcium wave, occurred once around RasV12 cells during the time-lapse observation (Figure S1F). The calcium wave was spread across 3-16 cell-length with a speed of 5-8 μm/s (Figures 1A, S1D, S1E, and S1G). The GCaMP6S fluorescence intensity was comparable between proximal and distal cells (Figures S1D and S1E), suggesting that the calcium wave is not mediated just by simple diffusion of calcium ion from RasV12 cells. This phenomenon occurred in about half of the RasV12 cells during the time-lapse observation (Figure 1E). In contrast, when mCherry alone was expressed, the calcium wave did not occur (Figures 1B, 1D, 1E, and Video S2). The calcium wave was not also observed when RasV12 cells alone were cultured (Video S3). Prior to calcium wave, no obvious morphological changes were observed in either RasV12 cells or the

surrounding cells (data not shown). When calcium wave occurred, RasV12 cells were apically extruded more frequently (Figure 1F). The xy-image analysis of apically extruding RasV12 cells demonstrated that just after calcium wave, the area of RasV12 cells started to decrease (Figures 1G, 1H, S1H, and S1I). Collectively, these data imply that calcium wave triggers and facilitates apical extrusion of RasV12-transformed cells.

IP_3 Receptor, Gap Junction, and Mechanosensitive Calcium Channel TRPC1 Are Involved in Calcium Wave

Intracellular calcium level can be regulated mainly by three channels: plasma membrane calcium channel, ER calcium channel, and gap junction. Then, we analyzed the effect of various channel inhibitors on calcium wave. Addition of GsMTx (mechanosensitive calcium channel inhibitor), Xestospongin C (Xesto) (IP_3 receptor inhibitor), or 18α-Glycyrrhetinic acid (αGA) (gap junction inhibitor) diminished the occurrence of calcium wave (Figures 2A, S2A, and S2B). Furthermore, GsMTx, Xesto, or αGA significantly suppressed apical extrusion of RasV12 cells (Figures 2B and 2C). In contrast, Amlodipine (Am) (L-type calcium channel inhibitor) or Dantrolene (Dan) (ryanodine receptor inhibitor) did not affect calcium wave or apical extrusion (Figures 2A and 2C). Knockdown of IP_3 receptor or gap junction protein connexin 43 suppressed the occurrence of calcium wave (Figures 2D-2F and S2B-S2E). These results indicate that mechanosensitive calcium channel, IP_3 receptor, and gap junction regulate these processes. A previous study has shown that during the extrusion of apoptotic cells, actomyosin rings form around the apoptotic cells, thereby producing contractile forces and driving the extrusion process [7]. We found that myosin-II accumulated around RasV12 cells at the final step of

apical extrusion (Figures S2F and S2G). Addition of Xesto substantially diminished the myosin ring formation (Figure S2H). Furthermore, the ROCK inhibitor Y27632 did not suppress calcium wave, but diminished apical extrusion of RasV12 cells (Figures S2B, S2I, and S2J). These results suggest that calcium wave acts upstream of myosin accumulation. GsMTx suppresses mechanosensitive calcium channels such as transient receptor potential (TRP) C1 and C6 channels. We then established MDCK-GCaMP6S cells stably expressing TRPC1-shRNA or TRPC6-shRNA (Figures S3A and S3B). When RasV12 expression was transiently induced in TRPC1-knockdown epithelia, either calcium wave or apical extrusion was substantially suppressed, but not when induced in TRPC6-knockdown epithelia (Figures 2G, 2H, and S2B). In addition, comparable effect of TRPC1-knockdown was also observed in another experimental condition where MDCK cells stably expressing RasV12 cells were surrounded by TRPC1-knockdown cells (Figures S3C-S3E); TRPC1-knockdown in the surrounding cells did not obviously affect the initial calcium pulse in RasV12 cells, but suppressed the following calcium wave propagation in the surrounding cells (Figure S3F and S3G). Knockdown of another mechanosensitive calcium channel Piezo1 did not affect calcium wave or apical extrusion (Figures S3H-S3K). These results indicate that TRPC1 plays a crucial role in the calcium propagation across the surrounding cells, which facilitates apical extrusion. Both IP_3R and TRPC1 are involved in store-operated calcium entry (SOCE), which is mediated by stromal interaction molecule (STIM) 1 that bridges the ER and plasma membranes [12-14]. The STIM1 inhibitor SKF96365 suppressed both calcium wave and apical extrusion (Figures 2I, 2J, and S3L), suggesting the involvement of SOCE in these processes.

Calcium Wave Precedes Apical Extrusion of RasV12-Transformed Cells in Zebrafish Embryos as Well

To demonstrate the prevalence of this phenomenon, we examined the involvement of calcium wave in apical extrusion of transformed cells in zebrafish embryos. In the outermost epithelial monolayer of embryos in late somitogenesis stages, the newly emerging mKO2-RasV12-expressing cells were apically extruded (Figures 3A and 3B). We found that prior to apical extrusion, the calcium wave was often propagated from RasV12 cells towards the surrounding epithelial cells (Figures 3C, 3D, S4A, S4B, and Videos S4). In about half of the cases, calcium wave occurred once during the time-lapse observation (Figure S4C) and was spread across 2-7 cell-length (Figure S4D). Upon calcium wave, the area of RasV12 cells abruptly decreased, accompanied by the morphological change into a round shape and the progression of apical extrusion (Figures 3C and 3E), compatible with the phenotypes observed in MDCK cells. When calcium wave occurred, apical extrusion of RasV12 cells was more frequently observed (Figure 3F). In contrast, expression of mKO2 alone did not induce calcium wave (Figure 3D and Video S5). Furthermore, addition of 2-aminoethoxydiphenylborane (2APB), the inhibitor for mechanosensitive calcium channel and IP_3 receptor, significantly suppressed calcium wave and apical extrusion of RasV12 cells (Figures 3A and 3B, and data not shown). Collectively, these data demonstrate that calcium wave is involved in apical elimination of transformed cells in zebrafish embryos as well.

Calcium Wave Induces the Polarized Movement of the Surrounding Cells toward the Extruding Transformed Cells during Apical Extrusion

Next, we explored the functional significance of calcium wave. While transformed cells are apically extruding, the surrounding cells fill the vacant space, but the underlying molecular mechanism of this process remains enigmatic. We then analyzed the movement of vertices of the surrounding cells that reside inside or outside of calcium wave; the displacement and direction of movement of cell vertices were quantified during apical extrusion (Figures 4A-4C). The vertices inside calcium wave moved further than those outside calcium wave (Figures 4D, 4E, and S5A). In addition, the vertices inside calcium wave moved preferentially toward the extruding transformed cell, whereas those outside calcium wave did not show the polarized movement (Figures 4F and S5B). The polarized movement of the surrounding cells continued until the completion of apical extrusion (Figures S5C and S5D). Furthermore, around the apically extruded cells without calcium wave, the polarized movement was less prominently observed (Figures S5E and S5F). Moreover, TRPC1-knockdown significantly diminished increased and polarized movement of vertices (Figures 4G-4I, S5A, and S5B). The displacement and direction of movement of cell vertices inside calcium wave showed correlation, which was diminished by TRPC1-knockdown (Figure S5G). These data suggest that calcium wave regulates the orchestrated movement of the surrounding cells during apical extrusion.

Calcium Wave Facilitates Apical Extrusion by Inducing Actin Rearrangement in the Surrounding Cells

Calcium signaling can influence actin cytoskeletons [15, 16]; therefore we examined the localization of F-actin during apical extrusion. We then observed that F-actin was often accumulated in the cytosol and perinuclear region in cells that surrounded apically extruding transformed cells, but not in those surrounding not-extruded

transformed cells (Figures 5A, 5B, and S6A). The F-actin accumulation in the cytosol and perinuclear region was observed in more than half of the cells that calcium wave had reached (Figure S6B). GsMTx treatment or TRPC1-knockdown significantly suppressed this actin phenotype (Figures 5C-5F). The actin phenotype was also diminished by the pan PKC inhibitor BIM-1 or the Ca^{2+}-dependent conventional PKC inhibitor Go6976, or the IP_3 receptor inhibitor Xesto (Figures 5G-5K). These data suggest that calcium signaling acts upstream of the actin rearrangement during apical extrusion. Previous studies have shown that increased intracellular calcium can induce perinuclear actin accumulation via inverted formin 2 (INF2) [15, 16]. Indeed, INF2-knockout profoundly diminished the actin phenotype around the apically extruding cells (Figures 6A-6D, and S6C). In addition, INF2-knockout significantly suppressed frequency of apical extrusion (Figure 6E). Even when apical extrusion of transformed cells occurred within INF2-knockout epithelia, the process of apical extrusion was prolonged (Figure 6F). Moreover, the polarized movement, but not the displacement, of the surrounding cells was significantly inhibited by INF2-knockout (Figures 6G and S6D). Collectively, these results imply that calcium wave facilitates apical extrusion, at least partly, by inducing actin rearrangement in the surrounding cells.

Calcium Wave Also Plays a Positive Role in Apical Extrusion of Apoptotic Cells

Previous studies have demonstrated that cells undergoing apoptosis are apically extruded from the epithelial layer [7, 17]. Thus, we examined whether calcium wave is also involved in apoptosis-mediated cell extrusion. Expression of the pro-apoptotic factor caspase-8 induced apoptosis within the MDCK epithelia (Figure 7A). At 15-70 min after caspase-8 expression, apoptotic cells were apically extruded from the epithelial layer. We observed that after induction of caspase-8 expression,

intracellular calcium was often elevated in a caspase-8-expressing cell, which was followed by explosive calcium wave across the surrounding cells (Figure 7B and Video S6). The calcium wave was observed in about 80% of caspase-8-expressing cells (Figure 7D). In contrast, calcium wave did not occur when mCherry alone was expressed (Figures 7C and 7D). Most of caspase-8-expressing cells eventually underwent apical extrusion irrespective of calcium wave, but upon calcium wave the extrusion time was substantially shortened after caspase-8 induction compared with when calcium wave did not occur (Figure 7E), suggesting that calcium wave facilitates the process of apoptosis-mediated cell extrusion, though not absolutely required for the occurrence of extrusion. Addition of GsMTx, Xesto, or αGA suppressed the frequency of calcium wave and prolonged the extrusion time after caspase-8 expression (Figures 7G and 7H), implying that common molecular machineries are, at least partly, involved in extrusion of both transformed and apoptotic cells. The vertex analyses showed that the vertices of cells inside calcium wave moved further and more preferentially toward apoptotic cells during apical extrusion (Figures 7I and 7J). Furthermore, the cytosolic and perinuclear accumulation of F-actin was frequently observed in the cells surrounding extruding apoptotic cells (Figures 7K and 7L). Moreover, calcium wave was also observed around laser-ablated dying cells in zebrafish embryos (Figure S7A and Video S7), which induced comparable effects on the movement of the surrounding cells (Figures S7B-S7D). Collectively, these results indicate that calcium wave also plays a positive role in apical extrusion of apoptotic cells.

DISCUSSION

In this study, we demonstrate that calcium wave promotes apical extrusion of transformed cells in both mammalian cultured cells and zebrafish embryos. In both experimental conditions, the calcium level is first elevated in transformed cells, and then calcium wave propagates across the surrounding cells. Calcium wave also plays a positive role in extrusion of apoptotic cells, and comparable molecular mechanisms are involved in both extrusion processes. However, apoptotic cells less depend on calcium wave for extrusion, and much more intense actomyosin rings are formed around apoptotic cells, compared with those around transformed cells (data not shown). This suggests the presence of additional, distinct mechanism(s) for apoptosis-mediated extrusion.

Addition of the IP_3 receptor inhibitor Xestospongin C or knockdown of IP_3 receptor suppresses both the initial calcium elevation in RasV12-transformed cells and the following calcium propagation across the surrounding cells. When RasV12 cells (with intact IP_3 receptor) are surrounded by IP_3 receptor-knockdown cells, calcium propagation is still suppressed, indicating that IP_3 receptor in both Ras cells and the surrounding cells is required for calcium wave. Furthermore, addition of the gap junction inhibitor αGA or knockdown of connexin 43 does not affect the initial calcium elevation in RasV12 cells, but blocks calcium propagation, demonstrating an essential role of gap junction in the latter process.

Either GsMTx treatment or TRPC1-knockdown suppresses both elevation of calcium in RasV12 cells and the following calcium propagation. Together with the data that the STIM1 inhibitor suppresses calcium wave, store-operated calcium entry (SOCE) plays a role in calcium propagation. In SOCE, Ca^{2+} is first released from the ER in response to activation of IP_3 receptor, which causes the conformational change

of ER-residing STIM1 and its recruitment into the plasma membrane that brings ER closer to plasma membrane. STIM1 then activates TRPC1 channel, resulting in the further elevation of the intracellular Ca^{2+} level [12-14]. In these processes, IP_3 is the key upstream regulator. As shown in Figures S1D and S1E, the calcium propagation is not caused just by simple diffusion of calcium ion, suggesting that other second messenger(s) may be also propagated through gap junction. It is thus plausible that during calcium wave, IP_3 is propagated through gap junction as proposed in another type of intercellular calcium wave [18, 19]. In addition, regarding the functional mode of TRPC1, TRPC1 might be activated not only by SOCE, but also by membrane stretching. Upon apical extrusion, non-cell-autonomous activation of myosin-II occurs in RasV12-transformed cells [1]. Similarly, actomyosin contraction is induced in apoptotic cells at the initial step of cell extrusion [7, 17, 20]. Then, contractile forces generated in extruding cells promote membrane stretching of the neighboring cells [21]. Thus, activity of TRPC1 may be also provoked by the stretching of the surrounding cells. These possibilities need to be further examined in future studies.

Intercellular calcium wave has been observed under various conditions [9]. In particular, the wound scratch within a cell monolayer induces calcium propagation from the wound, which resembles the cell extrusion-mediated calcium wave in certain aspects. For example, both processes involve the coordinated cell movement after calcium wave. In addition, IP_3 receptor and gap junction are involved in the propagation of calcium [19, 22, 23], though the involvement of gap junction in wound-mediated calcium wave remains controversial [22, 24, 25]. However, there are some differences between these two processes. First, the velocity of extrusion-mediated calcium wave is 5-8 μm/s, whereas that of wound-mediated calcium wave is 10-30 μm/s [24, 26]. Second, soluble factors from the wounded cells play a role in

wound-mediated calcium wave [22, 24, 27]. Third, upon wound-mediated calcium wave, perinuclear accumulation of actin filaments abruptly occurs, a process called calcium-mediated actin reset (CaAR) [15]. But, the mode of perinuclear F-actin accumulation seems different between wound healing and apical extrusion. In particular, during wound healing CaAR appears quite temporarily for just 2 min, whereas during apical extrusion perinuclear accumulation of F-actin can stay for much longer duration after calcium wave. Thus, the two types of calcium wave are governed by overlapping, but distinct molecular mechanisms.

Calcium signaling-mediated actin rearrangement promotes polarized movement of the surrounding cells during apical extrusion. However, the cytosolic and perinuclear F-actin do not show obvious planar-polarized localization. Thus, at present it is still unknown how the flow of calcium wave from extruding cells is converted into the polarized movement of the surrounding cells. Upon calcium wave, certain molecules or structures might be aligned or polarized toward the extruding cell; the functional roles of calcium wave remain to be further elucidated.

In summary, we demonstrate that calcium wave promotes apical extrusion of transformed and apoptotic cells in mammalian cultured cells and zebrafish embryos. Hence, calcium wave is an evolutionarily conserved, general regulatory mechanism of cell extrusion.

ACKNOWLEDGMENTS

We thank H. Nakano, J. Nakai, N. Kinoshita, and K. Kawakami for providing pcDNA3-HA-caspase-8, pCS2-GCaMP7, pCS2-Lifeact-GFP, and pT2 UAS mKO2-T2A-stop, respectively. We also thank K. Kawakami and H. Wada for the Tg[krt4:GAL4] line. This work was supported by Japan Society for the Promotion of Science (JSPS) Grant-in-Aid for Scientific Research (A) 18H03994, Strategic Japanese-Swiss Science and Technology Program, AMED under Grant Number JP19ck0106361h0003 and JP19cm0106234h0002, SAN-ESU GIKEN CO. LTD, and the Takeda Science Foundation (to Ya.F.); Grant-in-Aid for Young Scientists (B) 17K15113 and JSPS Fellows 16J00401 (to Y.T.); the Cancer Research UK A15936 (to M.T.); JSPS Research Fellowships for Young Scientists JP17J03677 (to Y.A.). In addition, Ya.F., T.I., T.M., and Y.O. were supported by Japan Society for the Promotion of Science (JSPS) Grant-in-Aid for Scientific Research on Innovative Areas 26114001.

AUTHOR CONTRIBUTIONS

Ya.T., R.N., and R.A. designed experiments and generated most of the data. T.S., N.T., K.K., S.I., and M.K. assisted experiments. M.T., Yu.H., Y.A., T.I., S.Y., and Yo.H. designed, performed, and analyzed zebrafish experiments. Yo.F. and Y.O. assisted imaging analyses. E.V. and Yu.T. assisted biophysical experiments. T.M. and Ya.F. conceived and designed the study. The manuscript was written by Ya.T., R.N., R.A., T.M., and Ya.F. with assistance from the other authors.

DECLARATION OF INTERESTS

The authors declare no competing interests.

FIGURE LEGENDS

Figure 1. Calcium Wave Precedes Apical Extrusion of RasV12-Transformed Cells

(A-D) Time-lapse analyses of calcium imaging of RasV12-expressing cells surrounded by normal epithelial cells. Myc-RasV12 and mCherry (A and C) or mCherry alone (B and D) were transiently expressed in a monolayer of MDCK-GCaMP6S cells. At 10 h after transfection, we performed time-lapse observation for 16 h. Images are extracted from a representative time-lapse analysis. The arrowheads indicate a RasV12 cell in which the initial elevation of calcium occurred. (C and D) The GFP intensity of GCaMP6S is quantified in mCherry-expressing cells (red line) or surrounding cells (green line). For surrounding cells, the average GFP intensity of cells directly contacting the mCherry-expressing cell is calculated. Values are expressed as a ratio relative to that at -3 min.

(E) Frequency of calcium wave around Myc-RasV12 cells. n=29 and 30 cells from three independent experiments. $^{\dagger\dagger}P < 0.005$ (chi-square test).

(F) Correlation between calcium wave and apical extrusion. n=35 and 148 cells from three independent experiments. $^{\dagger\dagger\dagger}P < 5 \times 10^{-14}$ (chi-square test).

(G and H) Reduction of area of an extruding MDCK-pTRE3G Myc-RasV12 cell after calcium wave. Myc-RasV12 cells stained with a red fluorescence dye CMTPX were co-cultured with MDCK-GCaMP6S cells at a ratio of 1:50. The dotted lines delineate the contour of an extruding Myc-RasV12 cell. Time 0 denotes the occurrence of calcium wave. Note that in this experiment, RasV12 cells did not express GCaMP6S.

(H) Data are from nine independent experiments. The data of Figure 1G is depicted in red line.

(A, B, and G) Scale bars, 50 μm.

See also Figure S1 and Videos S1-S3.

Figure 2. IP_3 Receptor, Gap Junction, and Mechanosensitive TRPC1 Channel Are Involved in Calcium Wave and Apical Extrusion

(A-C) Effect of various calcium channel inhibitors on calcium wave (A) or apical extrusion (B and C). Doxycycline-inducible MDCK-pTRE3G Myc-RasV12 cells stained with CMTPX (red) were co-cultured with MDCK-GCaMP6S cells at a ratio of 1:50 in the presence of doxycycline and the indicated inhibitor for 24 h. The following inhibitors suppress the respective calcium channels: Am (Amlodipine), L-type calcium channel; GsMTx, mechanosensitive calcium channel; Dan (Dantrolene), ryanodine receptor; Xesto (Xestospongin C), IP_3 receptor; αGA (18α-Glycyrrhetinic acid), GAP junction. (A) n=30, 51, 33, 32, 29, and 33 cells from three independent experiments. $^{\dagger}P < 0.05$, $^{\dagger\dagger}P < 0.01$, $^{\dagger\dagger\dagger}P < 0.001$ (chi-square test). (B) Fluorescence images of xz sections of Myc-RasV12 cells surrounded by normal cells. Scale bars, 20 μm. (C) Data are mean ± SD from three independent experiments. n≧50 cells for each experimental condition. *P<0.05, ***P<0.001 (two-tailed Student's t-tests).

(D) Effect of IP_3 receptor (IP_3R)-shRNA expression on the IP_3R mRNA level in MDCK-GCaMP6S cells. Data are mean ± SD from three independent experiments. *P<0.05, **P<0.01 (two-tailed Student's t-tests).

(E and F) Effect of IP_3R-knockdown on calcium wave. IP_3R was knocked down in both RasV12 and the surrounding cells in (E) or only in the surrounding cells in (F). (E) Expression of Myc-RasV12 was transiently induced in MDCK-GCaMP6S or MDCK-GCaMP6S IP_3R-shRNA1 cells. n=30 and 52 cells from three independent experiments. $^{\dagger}P < 0.05$ (chi-square test). (F) MDCK-pTRE3G Myc-RasV12 cells

were surrounded by MDCK-GCaMP6S or MDCK-GCaMP6S IP_3R-shRNA1 cells. n=30 and 60 cells from three independent experiments. $^{\dagger}P < 0.05$ (chi-square test). The comparable effect of IP_3R-knockdown on calcium wave was also observed using IP_3R-shRNA2 cells. Note that the expression level of IP_3R is not influenced by the RasV12 expression (data not shown).

(G and H) Effect of the transient receptor potential C1 (TRPC1)- or C6 (TRPC6)-knockdown on calcium wave (G) or apical extrusion (H). (G) n=30, 31, 32, 31, and 32 cells from three independent experiments. $^{\dagger\dagger}P < 0.01$ (chi-square test). (H) Data are mean ± SD from three independent experiments. n≧50 cells for each experimental condition. $^{**}P<0.01$, $^{***}P<0.001$ (two-tailed Student's *t*-test). In the following experiments, for TRPC1-knockdown cells, MDCK-GCaMP6S TRPC1-shRNA1 cells were used if not indicated.

(I and J) Effect of the STIM1 inhibitor SKF96365 (SKF) on calcium wave (I) or apical extrusion (J). (I) n=30 and 29 cells from three independent experiments. $^{\dagger}P < 0.05$ (chi-square test). (J) Data are mean ± SD from three independent experiments. n≧50 cells for each experimental condition. $^{***}P<0.001$ (two-tailed Student's *t*-test). See also Figure S2 and S3.

Figure 3. Calcium Wave Occurs Prior to Apical Extrusion in Zebrafish Embryos as Well

(A) Immunofluorescence images of zebrafish embryos in the absence or presence of 2-aminoethoxydiphenylborane (2APB), the inhibitor for mechanosensitive calcium channel and IP_3 receptor.

(B) Quantification of apical extrusion. Data are mean ± SD from three independent experiments. n≧50 cells for each experimental condition. *P<0.05 (two-tailed Student's t-tests).

(C) Time-lapse images of calcium wave from an extruding mKO2-RasV12-expressing cell in the enveloping layer of zebrafish embryos. Images were captured every 10.8 s.

(D) Frequency of calcium wave around mKO2-expressing cells. n=30 and 86 cells from 15 independent experiments. $^{\dagger}P < 0.05$ (chi-square test).

(E) Reduction of area of an extruding mKO2-RasV12 cell after calcium waves. The comparable area change of RasV12 cells after calcium wave has been observed in a well-reproducible manner.

(F) Correlation between calcium wave and apical extrusion. n=58 and 28 cells from 10 independent experiments. $^{\dagger\dagger\dagger}P < 0.001$ (chi-square test).

(A and C) Scale bars, 50 μm.

See also Figure S4, Videos S4 and S5.

Figure 4. Calcium Wave Induces the Polarized Movement of the Surrounding Cells toward the Extruding Transformed Cells

(A-D) Analyses of vertices of the surrounding cells that reside inside or outside of calcium wave during apical extrusion of Myc-RasV12-expressing cells. (A) Representative images of an extruding Myc-RasV12 cell stained with a blue fluorescence dye CMAC (left), calcium wave (center), and the far-red silicon rhodamine (SiR)-actin fluorescence probe (right). MDCK-pTRE3G Myc-RasV12 cells were co-cultured with MDCK-GCaMP6S cells with the SiR-actin probe. After incubation with doxycycline for 10 h, we performed time-lapse observation for 16 h.

Images are extracted from a representative time-lapse analysis. (B) Reduction of area of an extruding Myc-RasV12 cell after calcium wave. Time 0 denotes the occurrence of calcium wave. 'Start' represents the start of apical extrusion when the area reduction starts, whereas 'End' indicates the completion of apical extrusion when the area becomes zero. (C) Schematic diagram for the displacement and direction of movement of cell vertices during apical extrusion. The yellow arrow denotes the vertex movement from Start to End. Arrow angle (θ) is formed between the End and Start vertices, and the centroid of the extruding RasV12 cell. Arrow length and angle indicate the displacement and direction of the vertex movement, respectively. (D) Representative images of SiR-actin (Start). The white line indicates the border of calcium wave. The red dot (Border-In vertex) or blue dot (Border-Out vertex) is one-row inside or outside vertex from the border of calcium wave, respectively.
(E) Quantification of the displacement of the vertex movement. The displacement of each vertex movement is depicted as a dot. Data are mean ± SD. n=88 and 87 from three independent experiments. *P<0.05 (unpaired t-tests).
(F) Quantification of the direction of the vertex movement. Arrow angle (θ) was classified into 4 categories (0-45, 45-90, 90-135, 135-180), and the ratio of each category was quantified. Data are mean ± SD from three independent experiments. n=88 and 87 from three independent experiments. **P<0.01 (unpaired t-tests).
(G) Representative images of SiR-actin (Start). Images are extracted from a representative time-lapse analysis. MDCK-pTRE3G Myc-RasV12 cells stained with CMAC were co-cultured with MDCK-GCaMP6S or MDCK-GCaMP6S TRPC1-knockdown cells with the far-red silicon rhodamine (SiR)-actin fluorescence probe. After incubation with doxycycline for 10 h, we performed time-lapse observation for 16 h with doxycycline. Most of the analyzed Border-Inside vertices (red dots) reside

at 3-6 cells away from RasV12 cells; thus, comparable areas are selected for the analysis of TRPC1-knockdown (KD) cell vertices (green dots).

(H) Quantification of the displacement of the vertex movement. The displacement of each vertex movement is depicted as a dot. Data are mean ± SD. n=234, 397, and 233 from three independent experiments. **P*<0.05, ***P*<0.01 (unpaired *t*-tests).

(I) Quantification of the direction of the vertex movement. Data are mean ± SD from three independent experiments. n= 205, 220, and 362 from three independent experiments. **P*<0.05 (unpaired *t*-tests).

(A, D, and G) Scale bars, 50 μm.

See also Figure S5.

Figure 5. F-Actin Is Accumulated in the Cytosol and Perinuclear Region in Cells that Surround Apically Extruding RasV12-Transformed Cells

(A) Fluorescence images of F-actin (red) with Alexa-Fluor-568-conjugated phalloidin in the mixed culture of MDCK and MDCK-pTRE3G Myc-RasV12 cells in the absence or presence of doxycycline (DOX). Myc-RasV12 cells stained with CMFDA (green) were surrounded by normal MDCK cells. The status of Myc-RasV12 cells is not-extruded (left and center) or extruding (right).

(B) Quantification of the actin phenotype. The actin phenotype indicates the condition where F-actin accumulates at both cytosol and perinuclear region. Cells directly contacting Myc-RasV12 cells are examined. Data are mean ± SD from three independent experiments. n= 364, 293, and 377 from three independent experiments. ***P*<0.01 (two-tailed Student's *t*-tests).

(C-K) Effect of the mechanosensitive calcium channel inhibitor GsMTx (C and D), TRPC1-knockdownon (E and F), the PKC inhibitor BIM-1 or Go6976 (G-I), or the

IP_3 receptor inhibitor Xesto (Xestospongin C) (J and K) on the actin phenotype. MDCK-pTRE3G Myc-RasV12 cells stained with CMAC (blue) (C-F) or CMFDA (green) (G-K) were surrounded by MDCK-GCaMP6S cells.

(D, F, H, I, and K) Quantification of the actin phenotype. Data are mean ± SD from three independent experiments. (D) n= 248 and 197 from three independent experiments. $^{**}P<0.01$ (two-tailed Student's *t*-tests). (F) n= 341 and 507 from three independent experiments. $^{***}P<0.001$ (two-tailed Student's *t*-tests). (H) n= 362 and 325 from three independent experiments. $^{*}P<0.05$ (two-tailed Student's *t*-tests). (I) n= 312 and 65 from three independent experiments. $^{**}P<0.01$ (two-tailed Student's *t*-tests). (K) n= 226 and 157 from three independent experiments. $^{*}P<0.05$ (two-tailed Student's *t*-tests).

(A, C, E, G, and J) Scale bars, 10 μm.

See also Figure S6.

Figure 6. Effect of Knockout of Inverted Formin 2 (INF2) in the Surrounding Cells on the Actin Phenotype

(A and B) Establishment of MDCK-INF2-knockout cells. (A) MDCK-INF2-knockout mutant No.1 and No.2 are homologous recombination of the *INF2* gene. (B) Expression of INF2 was examined by western blotting with the indicated antibodies. Lane 1: MDCK; Lane 2: MDCK-INF2-knockout mutant No.1 (homo); Lane 3: MDCK-INF2-knockout mutant (hetero); Lane 4: MDCK-INF2-knockout mutant No.2 (homo). In the following experiments, for INF2-knockout cells, MDCK-GCaMP6S INF2-knockout mutant No.1 cells were used if not indicated.

(C) Effect of knockout of inverted formin 2 (INF2) in the surrounding cells on the actin phenotype. MDCK-pTRE3G Myc-RasV12 cells stained with CMFDA (green) were surrounded by MDCK or MDCK-INF2-knockout cells. Scale bars, 10 μm.

(D) Quantification of the actin phenotype. Cells directly contacting extruding Myc-RasV12 cells were examined. Data are mean ± SD from three independent experiments. n= 337 and 282 from three independent experiments. ***P<0.001 (two-tailed Student's *t*-tests).

(E) Effect of knockout of INF2 in the surrounding cells on apical extrusion of Myc-RasV12 cells. Data are mean ± SD from three independent experiments. n≧50 cells for each experimental condition. **P<0.01, ***P<0.001 (two-tailed Student's *t*-tests).

(F) Effect of knockout of INF2 in the surrounding cells on area reduction of extruding Myc-RasV12 cells. Area reduction was examined for Myc-RasV12 cells that were surrounded by MDCK-GCaMP6S (red line: n=7) or MDCK-GCaMP6S INF2-knockout cells (blue line: n=4). Time 0 denotes the point where the area reduction starts.

(G) Quantification of the direction of the vertex movement. Data are mean ± SD from three independent experiments. n= 220, 193, and 176 from three independent experiments. *P<0.05, **P<0.01 (unpaired *t*-tests).

See also Figure S6.

Figure 7. Calcium Wave Facilitates the Process of Apoptosis-Induced Cell Extrusion

(A) Fluorescence images of xz sections of an mCherry- or mCherry-caspase-8-expressing cell.

(B and C) Time-lapse analyses of calcium imaging of caspase-8-expressing cells surrounded by normal epithelial cells. mCherry-caspase-8 (B) or mCherry (C) was transiently expressed in a monolayer of MDCK-GCaMP6S cells. The GFP intensity of GCaMP6S is quantified in an mCherry-expressing cell (red line) or surrounding cells (green line). For surrounding cells, the average GFP intensity of cells directly contacting the mCherry-expressing cell is calculated. Values are expressed as a ratio relative to that at time 0.

(D) Frequency of calcium wave around caspase-8 cells. n=57 and 49 cells from three independent experiments. $^{\dagger\dagger\dagger}P < 0.001$ (chi-square test).

(E) Quantification of extruding time of apoptotic cells. Data are mean ± SD from three independent experiments. n=11 and 26 from three independent experiments. ***P<0.001 (unpaired t-tests).

(F) Reduction of area of an apically extruding caspase-8 cell after calcium wave. Time 0 denotes the occurrence of calcium wave.

(G and H) Effect of various calcium channel inhibitors on calcium wave (G) or extrusion time of apoptotic cells (H). The following inhibitors are used: Z-VAD-FMK, pan-caspase inhibitor; GsMTx, mechanosensitive calcium channel inhibitor; Xestospongin C (Xesto), IP_3 receptor inhibitor; αGA (18α-Glycyrrhetinic acid), GAP junction inhibitor. (G) n=33, 58, 74, 61, and 141 cells from three independent experiments. $^{\dagger\dagger}P < 0.01$, $^{\dagger\dagger\dagger}P < 0.001$ (chi-square test). (H) Data are mean ± SD. n=37, 63, 46, and 73 cells from three independent experiments. **P<0.01 (unpaired t-tests).

(I) Quantification of the displacement of the vertex movement. The displacement of each vertex movement is depicted as a dot. Data are mean ± SD. n=46 and 28 from three independent experiments. **P<0.01 (unpaired t-tests).

(J) Quantification of the direction of the vertex movement. Data are mean ± SD from three independent experiments. n= 101 and 62 from three independent experiments. ***P*<0.01 (unpaired *t*-tests).

(K) Fluorescence images of the actin phenotype (red) around extruding iRFP/caspase-8-expressing cells. iRFP alone or iRFP and caspase-8 were transiently expressed in a monolayer of MDCK cells.

(L) Quantification of the actin phenotype. Cells directly contacting iRFP-expressing cells were examined. Data are mean ± SD from three independent experiments. n= 112 and 135 cells from three independent experiments. ***P*<0.01 (Student *t*-tests).

Scale bars, 20 μm (A), 50 μm (B and C), and 10 μm (K).

See also Figure S7, Videos S6 and S7.

STAR METHODS

LEAD CONTACT AND MATERIALS AVAILABILITY

Further information and requests for resources and reagents should be directed to and will be fulfilled by the Lead Contact, Yasuyuki Fujita (yasu@igm.hokudai.ac.jp). This study did not generate new unique reagents. There are no restrictions on any data or materials presented in this paper.

EXPERIMENTAL MODEL AND SUBJECT DETAILS

Animals

Wild-type and the Tg[krt4:GAL4] line were used in this study. The Tg[krt4:GAL4] line was kindly provided by K. Kawakami and H. Wada [30]. All zebrafish experiments were performed with the approval of the Animal Studies Committees in the Nara Institute of Science and Technology, Gunma University, and/or Kyushu University.

Cell Lines

MDCK cell lines were used in this study. The parental MDCK cell was a gift from W. Birchmeier. Mycoplasma contamination was regularly tested for all cell lines in use using a commercially available kit (MycoAlert, Lonza). MDCK and MDCK-pTRE3G Myc-RasV12 cells were cultured as previously described [5]. To establish MDCK-GCAMP6S or MDCK-pTRE3G Myc-RasV12 GCAMP6S cells, MDCK or MDCK-pTRE3G Myc-RasV12 cells were transfected with PB-EF1-MCS-IRES-Neo-GCaMP6S by nucleofection (Nucleofector™ 2b Kit L, Lonza), followed by selection

in medium containing 800 μg ml^{-1} of G418 (Geneticin, Gibco). MDCK-GCaMP6S cells stably expressing IP_3R-shRNA, connexin 43-shRNA, TRPC1-shRNA, TRPC6-shRNA, or Piezo1-shRNA in a tetracycline-inducible manner were established as follows; IP_3R-shRNA oligonucleotides (IP_3R-shRNA1: 5'-CCGGGCAGATCTTCAAGTTGTTACTCGAGTAACAACTTGAAGATCTGCTTTTTG-3' and 5'-AATTCAAAAAGCAGATCTTCAAGTTGTTACTCGAGTAACAACTTGAAGATCTGC-3' or IP_3R-shRNA2: 5'-CCGGGCAATCACATGTGGAAATTCTCGAGAATTTCCACATGTGATTGCTTTTTG-3' and 5'-AATTCAAAAAGCAATCACATGTGGAAATTCTCGAGAATTTCCACATGTGATTGC-3') or connexin 43-shRNA oligonucleotides (connexin 43-shRNA1: 5'-CCGGAGGTACAAGTTGGTATTTACTCGAGTAAATACCAACTTGTACCTTTTTTG-3' and 5'-AATTCAAAAAAGGTACAAGTTGGTATTTACTCGAGTAAATACCAACTTGTACCT-3' or connexin 43-shRNA2: 5'-CCGGTACAAGCAGAGCAGTATAACTCGAGTTATACTGCTCTGCTTGTATTTTTG-3' and 5'-AATTCAAAAATACAAGCAGAGCAGTATAACTCGAGTTATACTGCTCTGCTTGTA-3') or TRPC1-shRNA oligonucleotides (TRPC1-shRNA1: 5'-CCGGGAGAAATGCTGTTACCATACTCGAGTATGGTAACAGCATTTCTCTTTTTG-3' and 5'-AATTCAAAAAGAGAAATGCTGTTACCATACTCGAGTATGGTAACAGCATTTCTC-3' or TRPC1-shRNA2: 5'-CCGGTGCTTAGTGCATCGTTATCCTCGAGGATAACGATGCACTAAGCATTT

TTG-3’ and 5’-
AATTCAAAAATGCTTAGTGCATCGTTATCCTCGAGGATAACGATGCACTA
AGCA-3’) or TRPC6-shRNA oligonucleotides (TRPC6-shRNA1: 5’-
CCGGGCTTCTAGCTATTAGTAAACTCGAGTTTACTAATAGCTAGAAGCTTT
TTG-3’ and 5’-
AATTCAAAAAGCTTCTAGCTATTAGTAAACTCGAGTTTACTAATAGCTAGA
AGC-3’ or TRPC6-shRNA2: 5’-
CCGGGCATAGTAAACAATCAAGTCTCGAGACTTGATTGTTTACTATGCTTT
TTG-3’ and 5’-
AATTCAAAAAGCATAGTAAACAATCAAGTCTCGAGACTTGATTGTTTACT
ATGC-3’) or Piezo1-shRNA oligonucleotides (Piezo1-shRNA1: 5’-
CCGGTACAAATTTGGGCTAGAGATACTCGAGTATCTCTAGCCCAAATTTGT
ATTTTTG-3’ and 5’-
AATTCAAAAATACAAATTTGGGCTAGAGATACTCGAGTATCTCTAGCCCA
AATTTGTA-3’ or Piezo1-shRNA2: 5’-
CCGGCACCGTCAAAGGCTACTATGACTCGAGTCATAGTAGCCTTTGACGG
TGTTTTTG-3’ and 5’-
AATTCAAAAACACCGTCAAAGGCTACTATGACTCGAGTCATAGTAGCCTT
TGACGGTG-3’) were cloned into the AgeI/EcoRI site of pLKO-TetOn-puro
(Addgene). MDCK-GCaMP6S cells were transfected with pLKO-TetOn IP_3R-
shRNA, connexin 43-shRNA, TRPC1-shRNA, TRPC6-shRNA, or Piezo1-shRNA,
followed by selection in medium containing 500 ng ml^{-1} of puromycin (Sigma-
Aldrich). For MDCK-pTRE3G Myc-RasV12 cells, 1 μg ml^{-1} of doxycycline (Sigma-
Aldrich) was used to induce RasV12 expression. For MDCK-GCaMP6S-pLKO-
TetOn IP_3R-shRNA, connexin 43-shRNA, TRPC1-shRNA, TRPC6-shRNA, or

Piezo1-shRNA cells, 2 μg ml^{-1} of tetracycline (Sigma-Aldrich) was used to induce expression of the respective shRNA. MDCK-GCaMP6S-pLKO-TetOn IP_3R-shRNA, connexin 43-shRNA, TRPC1-shRNA, TRPC6-shRNA, or Piezo1-shRNA cells were incubated with tetracycline for 48 h to induce sufficient knockdown prior to co-incubation with MDCK-pTRE3G Myc-RasV12 cells. To establish MDCK cells stably expressing MLC-GFP, MDCK cells were transfected with pEGFP-N1-MLC using Lipofectamine™ 2000 (Life Technologies) according to the manufacturer's instructions, followed by selection in medium containing 800 μg ml^{-1} of G418.

METHODS DETAILS

Antibodies, plasmids, and materials

The following antibodies were used in this study: mouse anti-β-actin (MAB1501R clone C4) antibody from Millipore, rabbit anti-INF2 antibody (20466-1-AP) from Proteintech, and rabbit anti-cleaved caspase-3 (Asp175) antibody from Cell Signaling. Alexa-Fluor-568- and -647-conjugated phalloidin (Life Technologies) were used at 1.0 U ml^{-1}. Hoechst 33342 (Life Technologies) was used at a dilution of 1:5,000 for fluorescence and scratch assay. pGP-CMV-GCaMP6S and iRFP-C1 were obtained from Addgene. To construct pcDNA4-TO-mCherry-caspase-8, the cDNA of caspase-8 was excised from pcDNA3-HA-caspase-8 (gift from H. Nakano) and inserted into the HindⅢ/NotI site of pcDNA4-TO-mCherry [2]. To generate PB-EF1-MCS-IRES-Neo-GCaMP6S, the cDNA of GCAMP6S was excised from pGP-CMV-GCaMP6S and cloned into the BamHI/EcoRI site of pPB-TRE3G-MCS-CEH-rtTA3-IP [5]. pEGFPN1-MLC (myosin-II light chain) was a gift from H. Hosoya [28]. The inhibitors Amlodipine besylate (25 μM), α-Glycyrrhetinic acid (50 μM), and Go6976

(10 μM) were from Sigma-Aldrich. GsMTx (10 μM) was from PEPTIDE INSTITUTE, Inc. Xestospongin C (20 μM) and Ionomycin (2 μM) were from FUJIFILM WAKO Pure Chemical Corporation. Dantrolene (10 μM) and SKF96365 (50 μM) were from Santa Cruz Biochemistry. 2-aminoethoxydiphenylborane (2APB) (6.25 μM) was from Sigma-Aldrich. Thapsigargin (10 μM) was from Cayman CHEMICAL. Y27632 (20 μM), Bisindolylmaleimide (BIM)-I (10 μM), and Z-VAD-FMK (100 μM) were from Calbiochem. The Lucifer Yellow Probe (25 μM) for scratch assay was obtained from Molecular probes. Type I collagen (Cellmatrix® Type I-A) was obtained from Nitta Gelatin and was neutralized on ice to a final concentration of 2 mg ml^{-1} according to the manufacturer's instructions. The CellTracker dyes CMTPX (red), CMFDA (green), and CMAC (blue) (Life Technologies) were used according to the manufacturer's instructions. The SiR-actin Kit (far-red silicon rhodamine (SiR)-actin fluorescence probe) was obtained from SPIROCHROME for live imaging of F-actin and was used according to the manufacturer's instructions.

Cell culture

For the induction of caspase-8, MDCK or MDCK-GCaMP6S cells were transfected with pcDNA4-TO-mCherry-caspase-8 or co-transfected with pcDNA3-HA-caspase-8 and iRFP-C1 using Lipofectamine™ 2000. For analyses of calcium wave, apical extrusion, and actin phenotype, cells were incubated with the indicated inhibitor for 24 h. For scratch assay, cells were pre-incubated in medium containing Lucifer yellow and Hoechst for 15 min. At 10 min after scratching, they were observed by the Olympus FV1000 system.

CRISPER/Cas9-based generation of INF2-knockout cells

Guide sequences of INF2 single-guide RNA (sgRNA) targeting *Canis INF2* were designed on exon 1, as described previously [5]. INF2 sgRNA sequence (5'-CCCTCTGTGGTCAACTACTCGG-3') was introduced into the pCDH-EF1-Hygro-sgRNA vector. First, MDCK cells were infected with lentivirus carrying pCW-Cas9 and cultured in medium containing 500 ng ml^{-1} of puromycin. Tetracycline-inducible MDCK-Cas9 cells were pre-incubated with 2 μg ml^{-1} of tetracycline and transfected with pCDH-EF1-INF2 sgRNA by nucleofection, followed by selection in medium containing 200 μg ml^{-1} of hygromycin. Indels on the INF2 exon in each monoclone were analysed by direct sequencing using following primers (5'-GGAAAGGACGAAACACCGCCCTCTGTGGTCAACTACTGTTTTAGAGCTAG AAATAGC-3' and 5'-GCTATTTCTAGCTCTAAAACAGTAGTTGACCACAGAGGGCGGTGTTTCGTC CTTTCC-3'). To generate INF2-deleted cells carrying GCaMP6S, PB-EF1-MCS-IRES-Neo-GCaMP6S was introduced into the INF2-deleted cells by nucleofection, followed by selection in medium containing 800 μg ml^{-1} of G418.

Immunofluorescence and western blotting

For immunofluorescence, MDCK-pTRE3G Myc-RasV12 cells were mixed with MDCK, MDCK-GCaMP6S, MDCK-INF2-knockout, MDCK-GCaMP6S-pLKO-TetOn TRPC1-shRNA, TRPC6-shRNA, or Piezo1-shRNA cells at a ratio of 1:50 and plated onto collagen-coated coverslips as previously described [1]. The mixture of cells was incubated for 8–12 h, followed by doxycycline treatment for 16 h, except for analyses of apical extrusions that were examined after 24 h of doxycycline addition. Cells were fixed with 4% paraformaldehyde (PFA) in PBS and permeabilized as

previously described [2]. Primary antibodies were used at 1:100, and all secondary antibodies were used at 1:200. Immunofluorescence images were analyzed with the Olympus FV1000 or FV1200 system and Olympus FV10-ASW software. Images were quantified with the Metamorph software (Molecular Devices). For quantification of apical extrusion of RasV12-transformed cells, 2-8 RasV12-transformed cells that were surrounded by normal epithelial cells were analyzed. More than 50 cells of RasV12-transformed cells were analyzed for each condition. The ratio of apically extruded RasV12-transformed cells was quantified. The frequency of actin phenotype is calculated by the ratio of cells that exhibited the actin phenotype among cells adjacent to extruding Myc-RasV12 cells. Western blotting was carried out as previously described [29]. Primary antibodies were used at 1:1000. Western blotting data were analyzed using ImageQuant™ LAS4010 (GE Healthcare).

Quantitative real-time PCR

MDCK-GCaMP6S-pLKO-TetOn IP_3R-shRNA, connexin 43-shRNA, TRPC1-shRNA, TRPC6-shRNA, or Piezo1-shRNA cells were cultured on 6-well plates (Corning). After incubation with tetracycline for 48 h, total RNA was extracted using Trizol (Thermo Fisher Scientific) and a RNeasy Mini Kit (QIAGEN) and reverse-transcribed using a QuantiTect Reverse Transcription Kit (QIAGEN). GeneAce SYBR qPCR Mix (NIPPON GENE) was used to perform qPCR using the StepOne system (Thermo Fisher Scientific). For data analysis, relative quantification analysis was performed using the comparative CT ($2^{-\Delta\Delta CT}$) method. For each sample, the mRNA level of IP_3R, connexin 43, TRPC1, TRPC6, or Piezo1 was normalized to the β-actin mRNA. The primer sequences were as follows. IP_3R: 5'-TTGTCAGTCTGGTGCGAAAG-3' and 5'-AGAGCCACACCTCCTCTTCA-3';

connexin 43: 5’-GGACATGCACTTGAAGCAGA-3’ and 5’-ATGAGGGCAGGGTTCTCTTT-3’; TRPC1: 5’-CATGAGGCAGAAGATGCAAA-3’ and 5’-TGCAAATGCAGTCTTTCAGG-3’; TRPC6: 5’-GCCAATGAGCATCTGGAAAT-3’ and 5’-GCTGGTTGCTAACCTCTTGC-3’; Piezo1: 5’-CTTCCTGCTGGCACTCCTAC-3’ and 5’-CAGTGACCATGTGGTTGAGG -3’; β-actin: 5’-GGCACCCAGCACAATGAAG-3’ and 5’-ACAGTGAGGCCAGGATGGAG-3’.

Time-lapse observation of cultured cells

For live imaging, cells were incubated in Leibovitz’s medium (L-15) (Gibco) containing 10% fetal bovine serum (Sigma-Aldrich). For the quantification of calcium wave and area of MDCK-pTRE3G Myc-RasV12 cells, MDCK-GCaMP6S cells were mixed with Myc-RasV12 cells stained with CMTPX (red) at a ratio of 50:1 and seeded on the collagen-coated 35-mm glass bottom dish (Matsunami). The mixture of cells was incubated for 12-16 h until a monolayer was formed, followed by doxycycline treatment for 12 h. Then, they were observed for 8 h by Olympus epi-fluorescent microscopy (IX-81-ZDC-Meta). For the quantification of the occurrence of calcium wave, 1-4 RasV12-transformed cells that were surrounded by normal epithelial cells were analyzed. The percentage of the occurrence of calcium wave during timelapse-observation was quantified. For analyses of caspase-8-induced apoptosis, timing of mCherry-caspase-8 expression was determined when the mCherry intensity exceeded 1.1 times as the basal level. Apoptotic extrusion was determined by the obvious morphological change using bright field images of time-lapse observation.

For analyses of vertex movement of the surrounding cells, MDCK-GCaMP6S cells, MDCK-GCaMP6S TRPC1-knockdown cells, or MDCK-GCaMP6S INF2-knockout cells were mixed with Myc-RasV12 cells stained with CMAC (blue) at a ratio of 50:1 and seeded on the collagen-coated 35-mm glass bottom dishes. After 6 h, they were incubated in medium containing the far-red silicon rhodamine (SiR)-actin fluorescence probes for 24 h until time-lapse observation started. Doxycycline was added 10 h before the start of time-lapse imaging. We then performed time-lapse observation for 16 h. For analyses of the actin phenotype using grid-chamber dishes, MDCK-GCaMP6S cells were mixed with Myc-RasV12 cells stained with CMAC (blue) at a ratio of 50:1 and seeded on the collagen-coated 35-mm glass base dish with grid (Iwaki), followed by time-lapse analysis as described above. Time-lapse images were captured and analyzed by Nikon confocal microscopy (A1 HD25) with the NIS-Elements software (Nikon). Acquired data were analyzed by the Metamorph and ImageJ software.

Zebrafish

pCS2-GCaMP7 (gift from J. Nakai), pCS2-Lifeact-GFP (gift from N. Kinoshita), and pmtb-t7-alpha-bungarotoxin were used as templates for mRNA synthesis. mRNAs of GCaMP7, Lifeact-GFP, or bungarotoxin were synthesized using the SP6 mMessage mMachine System (Thermo Fisher Scientific). To observe calcium wave during apical extrusion from the outermost epithelial monolayer in zebrafish embryos, GCaMP7 mRNA (200 pg), pT2 UAS mKO2-T2A-RasV12 DNA (25 pg), and bungarotoxin mRNA (25 pg) were co-injected into the yolk of one-cell-stage embryos obtained by mating of the Tg[krt4:GAL4] line with wild-type zebrafish. When injected embryos were developed until late somitogenesis stages, embryos carrying

RasV12-transformed cells mosaically in the outermost epithelial monolayer were selected by confirming mosaic expression of mKO2 fluorescent proteins under the SZX16 stereomicroscope (Olympus). Selected embryos were dechorionated and mounted in holes of a gel made with 1% low-melting point agarose (Nacalai Tesque) on 35-mm glass bottom dishes (Greiner Bio-One). Calcium waves around mKO2-positive transformed cell(s) were observed with a confocal microscope (LSM710, LSM700, or LSM7 Duo, Zeiss) by 9-10 h time-lapse imaging at 9-12-s intervals. In each time point of the time-lapse, Z-stack images of the embryos (5-7 planes at 9-11-μm intervals) were obtained. For control, pT2 UAS mKO2-T2A-stop DNA (25 pg) was co-injected with mRNAs of GCaMP7 and bungarotoxin. pT2 UAS mKO2-T2A-stop was a kind gift from K. Kawakami [31]. To analyze apical extrusion, Lifeact-GFP mRNA (100 pg) and pT2 UAS mKO2-T2A-RasV12 DNA (25 pg) were co-injected into the yolk of one-cell-stage embryos obtained by mating of Tg[krt4:GAL4] with wild-type zebrafish. Injected embryos were developed until bud stage (10 hpf), treated with 6.25 μM 2APB or 0.25% DMSO for 12 h, and then fixed with 4% PFA in PBS. Z-stack images (5-10 planes at 1-2-μm intervals) were obtained with the Olympus FV1000 or FV1200 system and Olympus FV10-ASW software.

For laser ablation experiments, Tg[krt4:Lifeact GFP] embryos were injected with GCaMP7 mRNA and developed at around 6 hpf. A single shot of 800-nm laser pulse (100 fs, 200 nJ/pulse) from a Ti: sapphire femtosecond laser amplifier (Spectra-Physics) was focused into the center of epithelial cells in the enveloping layer through a 40×/NA0.8 objective lens (Olympus) [32]. Dynamic changes of F-actin and calcium were observed with a confocal microscope (FV300, Olympus) for 5-10 min at 1-s intervals. As reported in a previous study [33], DNA strand breaks were induced by irradiation of femtosecond laser in the nucleus of the cells, leading to apoptosis-like

cell death. Indeed, we observed cell blebbing after the laser irradiation. In addition, we have not observed any membrane rupture or cell fragmentation that often occurs during necrotic cell death.

QUANTIFICATION AND STATISTICAL ANALYSIS

Statistical analysis

For data analyses, Chi-square test, unpaired *t*-test, two-tailed Student's *t*-test, or two-tailed Pearson *r* correlation was used to determine *p* values. *p* values less than 0.05 were considered to be statistically significant.

DATA AND CODE AVAILABILITY

This study did not generate any unique datasets or code.

SUPPLEMENTAL VIDEO LEGENDS

Video S1. Calcium Wave Occurs from a RasV12-Transformed Cell and Propagates across the Surrounding Normal Cells in an Explosive Fashion. Related to Figure 1.

Figure 1A shows cropped images from the first video. The asterisk indicates a Myc-RasV12-expressing cell from which calcium wave originates. Images were captured at 5-s intervals.

Video S2. Calcium Wave does not Occur from an mCherry-Expressing Cell. Related to Figure 1.

Figure 1B shows cropped images from this video. The asterisk indicates an mCherry-expressing cell. Images were captured at 5-s intervals.

Video S3. Calcium Wave does not Occur When RasV12-Transformed Cells Alone Are Cultured. Related to Figure 1.

Images were captured at 5-s intervals.

Video S4. Calcium Wave Occurs from a RasV12-Transformed Cell in Zebrafish Embryos. Related to Figure 3.

The first, second, and third videos are shown as cropped images in Figures 3C, S4A, and S4B, respectively. The arrow indicates a RasV12-expressing cell from which calcium wave originates. Images were captured at 11-s intervals.

Video S5. Calcium Wave does not Occur from mKO2-Expressing Cells in Zebrafish Embryos. Related to Figure 3.

Calcium wave is not observed around mKO2-expressing cells. Images were captured at 11-s intervals.

Video S6. Calcium Wave Occurs from a Caspase-8-Expressing Cell.

Figure 7B shows cropped images from this video. The asterisk indicates a caspase-8-expressing cell from which calcium wave originates. Images were captured at 30-s intervals. **Related to Figure 7.**

Video S7. Calcium Wave Occurs around a Laser-Ablated Apoptotic Cell in Zebrafish Embryos. Related to Figure 7.

Figure S7A shows cropped images from this video. The asterisk indicates a laser-ablated cell from which calcium wave originates. Images were captured at 2-s intervals.

REFERENCES

1. Hogan, C., Dupre-Crochet, S., Norman, M., Kajita, M., Zimmermann, C., Pelling, A.E., Piddini, E., Baena-Lopez, L.A., Vincent, J.P., Itoh, Y., et al. (2009). Characterization of the interface between normal and transformed epithelial cells. Nat Cell Biol *11*, 460-467.
2. Kajita, M., Hogan, C., Harris, A.R., Dupre-Crochet, S., Itasaki, N., Kawakami, K., Charras, G., Tada, M., and Fujita, Y. (2010). Interaction with surrounding normal epithelial cells influences signalling pathways and behaviour of Src-transformed cells. J Cell Sci *123*, 171-180.
3. Leung, C.T., and Brugge, J.S. (2012). Outgrowth of single oncogene-expressing cells from suppressive epithelial environments. Nature *482*, 410-413.
4. Wu, S.K., Gomez, G.A., Michael, M., Verma, S., Cox, H.L., Lefevre, J.G., Parton, R.G., Hamilton, N.A., Neufeld, Z., and Yap, A.S. (2014). Cortical F-actin stabilization generates apical-lateral patterns of junctional contractility that integrate cells into epithelia. Nat Cell Biol *16*, 167-178.
5. Kon, S., Ishibashi, K., Katoh, H., Kitamoto, S., Shirai, T., Tanaka, S., Kajita, M., Ishikawa, S., Yamauchi, H., Yako, Y., et al. (2017). Cell competition with normal epithelial cells promotes apical extrusion of transformed cells through metabolic changes. Nat Cell Biol *19*, 530-541.
6. Sasaki, A., Nagatake, T., Egami, R., Gu, G., Takigawa, I., Ikeda, W., Nakatani, T., Kunisawa, J., and Fujita, Y. (2018). Obesity Suppresses Cell-Competition-Mediated Apical Elimination of RasV12-Transformed Cells from Epithelial Tissues. Cell Rep *23*, 974-982.
7. Rosenblatt, J., Raff, M.C., and Cramer, L.P. (2001). An epithelial cell destined for apoptosis signals its neighbors to extrude it by an actin- and myosin-dependent mechanism. Curr Biol *11*, 1847-1857.
8. Berridge, M.J., Bootman, M.D., and Roderick, H.L. (2003). Calcium signalling: dynamics, homeostasis and remodelling. Nat Rev Mol Cell Biol *4*, 517-529.
9. Leybaert, L., and Sanderson, M.J. (2012). Intercellular Ca(2+) waves: mechanisms and function. Physiol Rev *92*, 1359-1392.
10. Nakai, J., Ohkura, M., and Imoto, K. (2001). A high signal-to-noise Ca(2+) probe composed of a single green fluorescent protein. Nat Biotechnol *19*, 137-141.
11. Chen, T.W., Wardill, T.J., Sun, Y., Pulver, S.R., Renninger, S.L., Baohan, A., Schreiter, E.R., Kerr, R.A., Orger, M.B., Jayaraman, V., et al. (2013). Ultrasensitive fluorescent proteins for imaging neuronal activity. Nature *499*, 295-300.
12. Ambudkar, I.S., de Souza, L.B., and Ong, H.L. (2017). TRPC1, Orai1, and STIM1 in SOCE: Friends in tight spaces. Cell Calcium *63*, 33-39.
13. Prakriya, M., and Lewis, R.S. (2015). Store-Operated Calcium Channels. Physiol Rev *95*, 1383-1436.
14. Cahalan, M.D. (2009). STIMulating store-operated Ca(2+) entry. Nat Cell Biol *11*, 669-677.
15. Wales, P., Schuberth, C.E., Aufschnaiter, R., Fels, J., Garcia-Aguilar, I., Janning, A., Dlugos, C.P., Schafer-Herte, M., Klingner, C., Walte, M., et al. (2016). Calcium-mediated actin reset (CaAR) mediates acute cell adaptations. eLife *5*.

16. Shao, X., Li, Q., Mogilner, A., Bershadsky, A.D., and Shivashankar, G.V. (2015). Mechanical stimulation induces formin-dependent assembly of a perinuclear actin rim. Proc Natl Acad Sci U S A *112*, E2595-2601.
17. Kuipers, D., Mehonic, A., Kajita, M., Peter, L., Fujita, Y., Duke, T., Charras, G., and Gale, J.E. (2014). Epithelial repair is a two-stage process driven first by dying cells and then by their neighbours. J Cell Sci *127*, 1229-1241.
18. Sanderson, M.J., Charles, A.C., Boitano, S., and Dirksen, E.R. (1994). Mechanisms and function of intercellular calcium signaling. Mol Cell Endocrinol *98*, 173-187.
19. Sneyd, J., Wetton, B.T., Charles, A.C., and Sanderson, M.J. (1995). Intercellular calcium waves mediated by diffusion of inositol trisphosphate: a two-dimensional model. Am J Physiol *268*, C1537-1545.
20. Teng, X., Qin, L., Le Borgne, R., and Toyama, Y. (2017). Remodeling of adhesion and modulation of mechanical tensile forces during apoptosis in Drosophila epithelium. Development *144*, 95-105.
21. Lubkov, V., and Bar-Sagi, D. (2014). E-cadherin-mediated cell coupling is required for apoptotic cell extrusion. Curr Biol *24*, 868-874.
22. Shabir, S., and Southgate, J. (2008). Calcium signalling in wound-responsive normal human urothelial cell monolayers. Cell Calcium *44*, 453-464.
23. Xu, S., and Chisholm, A.D. (2011). A Galphaq-Ca(2)(+) signaling pathway promotes actin-mediated epidermal wound closure in C. elegans. Curr Biol *21*, 1960-1967.
24. Hinman, L.E., Beilman, G.J., Groehler, K.E., and Sammak, P.J. (1997). Wound-induced calcium waves in alveolar type II cells. Am J Physiol *273*, L1242-1248.
25. Klepeis, V.E., Cornell-Bell, A., and Trinkaus-Randall, V. (2001). Growth factors but not gap junctions play a role in injury-induced Ca2+ waves in epithelial cells. J Cell Sci *114*, 4185-4195.
26. Sammak, P.J., Hinman, L.E., Tran, P.O., Sjaastad, M.D., and Machen, T.E. (1997). How do injured cells communicate with the surviving cell monolayer? J Cell Sci *110 (Pt 4)*, 465-475.
27. Sung, Y.J., Sung, Z., Ho, C.L., Lin, M.T., Wang, J.S., Yang, S.C., Chen, Y.J., and Lin, C.H. (2003). Intercellular calcium waves mediate preferential cell growth toward the wound edge in polarized hepatic cells. Exp Cell Res *287*, 209-218.
28. Kajita, M., Sugimura, K., Ohoka, A., Burden, J., Suganuma, H., Ikegawa, M., Shimada, T., Kitamura, T., Shindoh, M., Ishikawa, S., et al. (2014). Filamin acts as a key regulator in epithelial defence against transformed cells. Nature communications *5*, 4428.
29. Hogan, C., Serpente, N., Cogram, P., Hosking, C.R., Bialucha, C.U., Feller, S.M., Braga, V.M., Birchmeier, W., and Fujita, Y. (2004). Rap1 regulates the formation of E-cadherin-based cell-cell contacts. Mol Cell Biol *24*, 6690-6700.
30. Wada, H., Ghysen, A., Asakawa, K., Abe, G., Ishitani, T., and Kawakami, K. (2013). Wnt/Dkk negative feedback regulates sensory organ size in zebrafish. Curr Biol *23*, 1559-1565.
31. Asakawa, K., Suster, M.L., Mizusawa, K., Nagayoshi, S., Kotani, T., Urasaki, A., Kishimoto, Y., Hibi, M., and Kawakami, K. (2008). Genetic dissection of neural circuits by Tol2 transposon-mediated Gal4 gene and enhancer trapping in zebrafish. Proc Natl Acad Sci U S A *105*, 1255-1260.

32. Yamada, S., Iino, T., Bessho, Y., Hosokawa, Y., and Matsui, T. (2017). Quantitative analysis of mechanical force required for cell extrusion in zebrafish embryonic epithelia. Biol Open *6*, 1575-1580.
33. Tirlapur, U.K., Konig, K., Peuckert, C., Krieg, R., and Halbhuber, K.J. (2001). Femtosecond near-infrared laser pulses elicit generation of reactive oxygen species in mammalian cells leading to apoptosis-like death. Exp Cell Res *263*, 88-97.

Figure 1

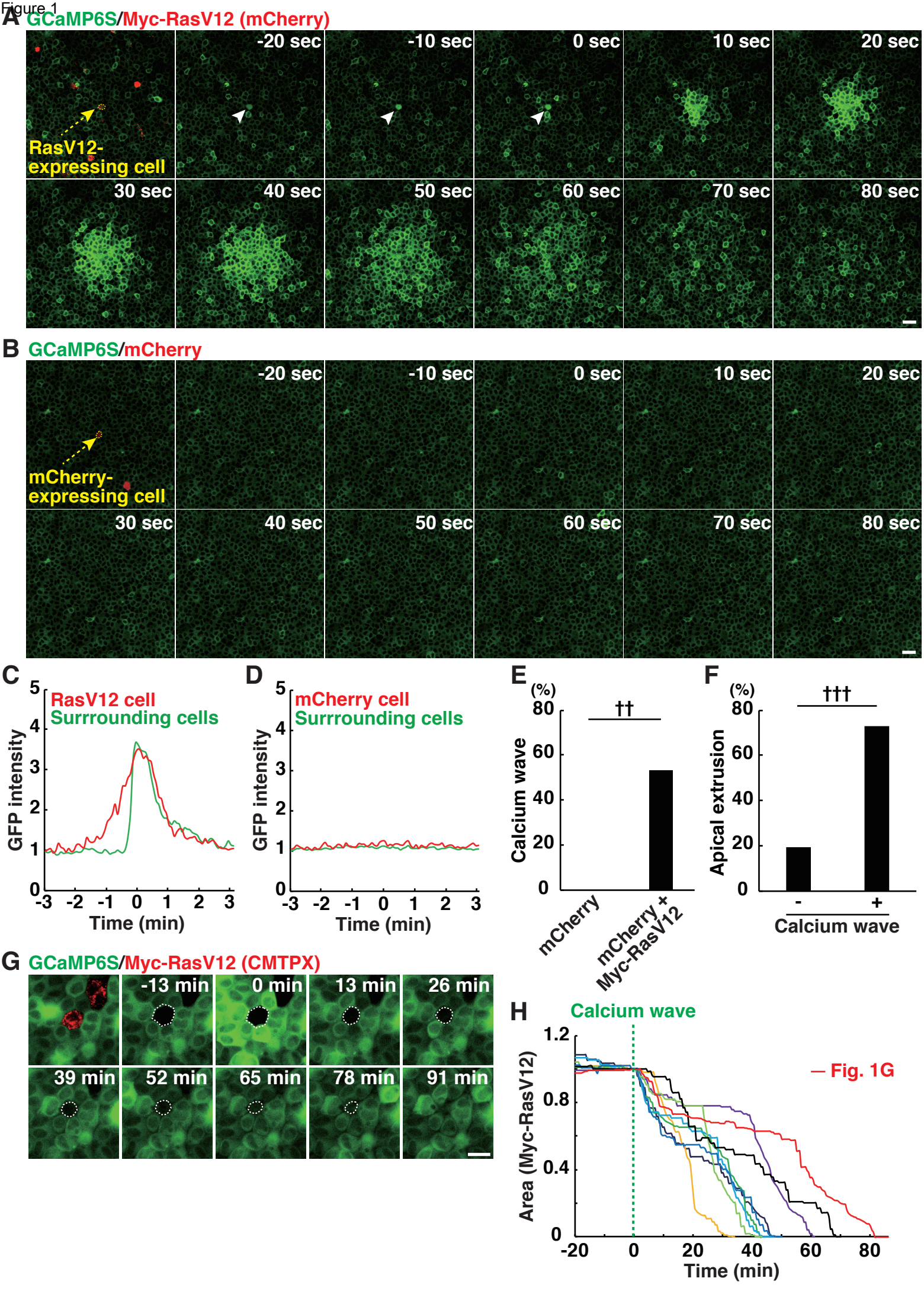

Figure 1 Takeuchi et al.

Figure 2

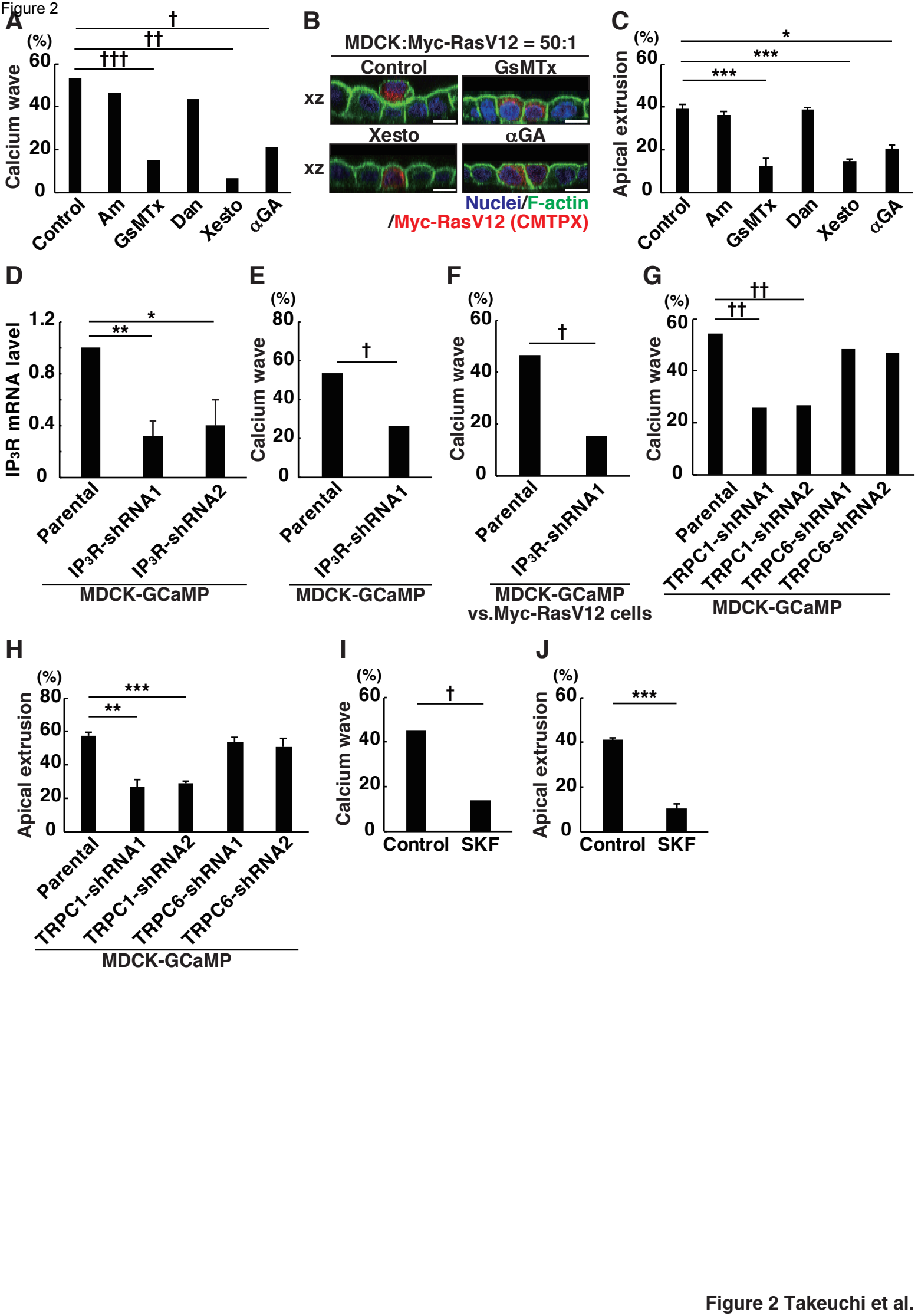
A
(%)
Calcium wave
Control
Am
GsMTx
Dan
Xesto
αGA
B
MDCK:Myc-RasV12 = 50:1
Control
GsMTx
Xesto
αGA
xz
Nuclei/F-actin
/Myc-RasV12 (CMTPX)
C
Apical extrusion
D
IP3R mRNA lavel
Parental
IP3R-shRNA1
IP3R-shRNA2
MDCK-GCaMP
E
Calcium wave
F
MDCK-GCaMP
vs.Myc-RasV12 cells
G
TRPC1-shRNA1
TRPC1-shRNA2
TRPC6-shRNA1
TRPC6-shRNA2
H
Apical extrusion
I
Control
SKF
J

Figure 3

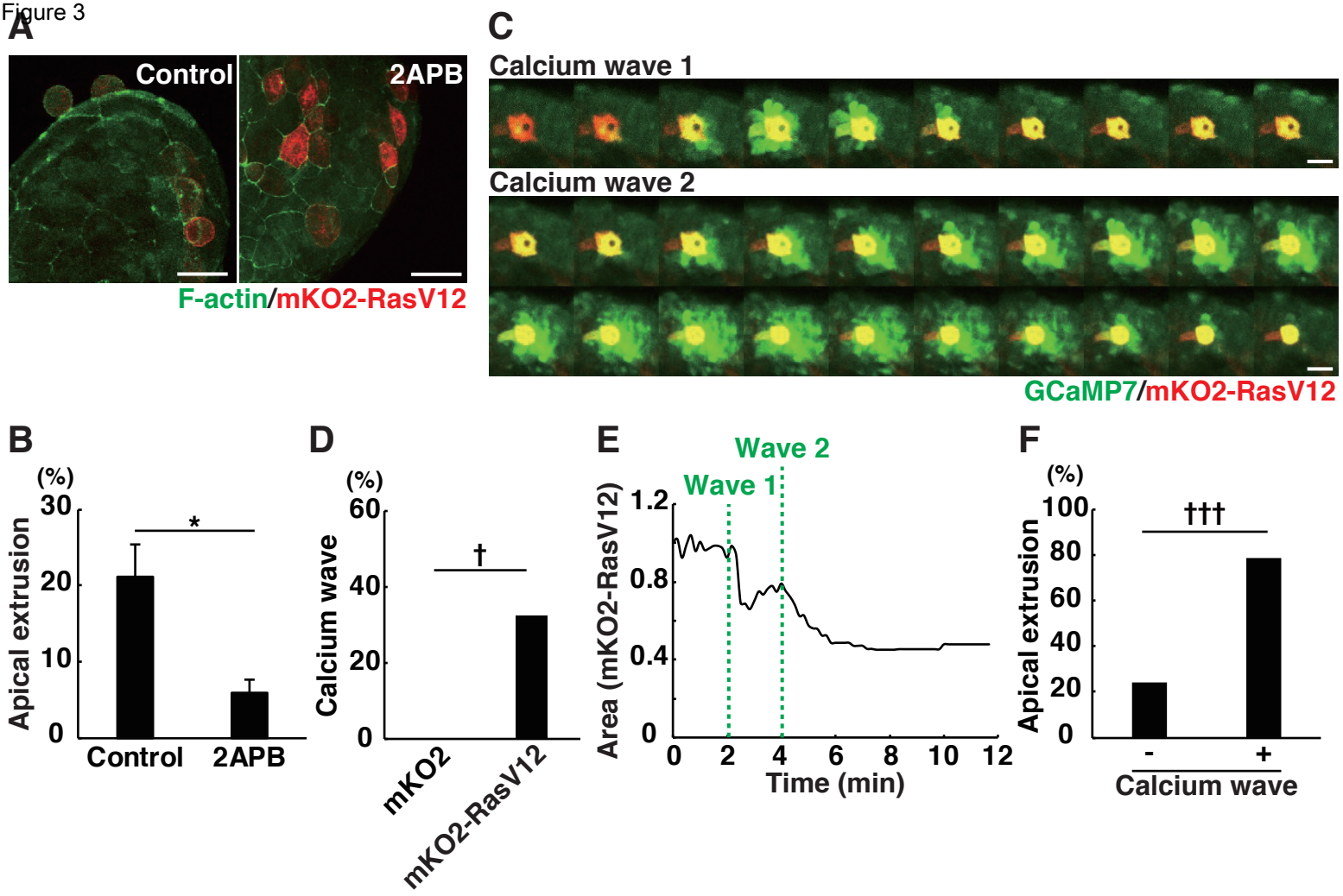

Figure 3 Takeuchi et al.

Figure 4

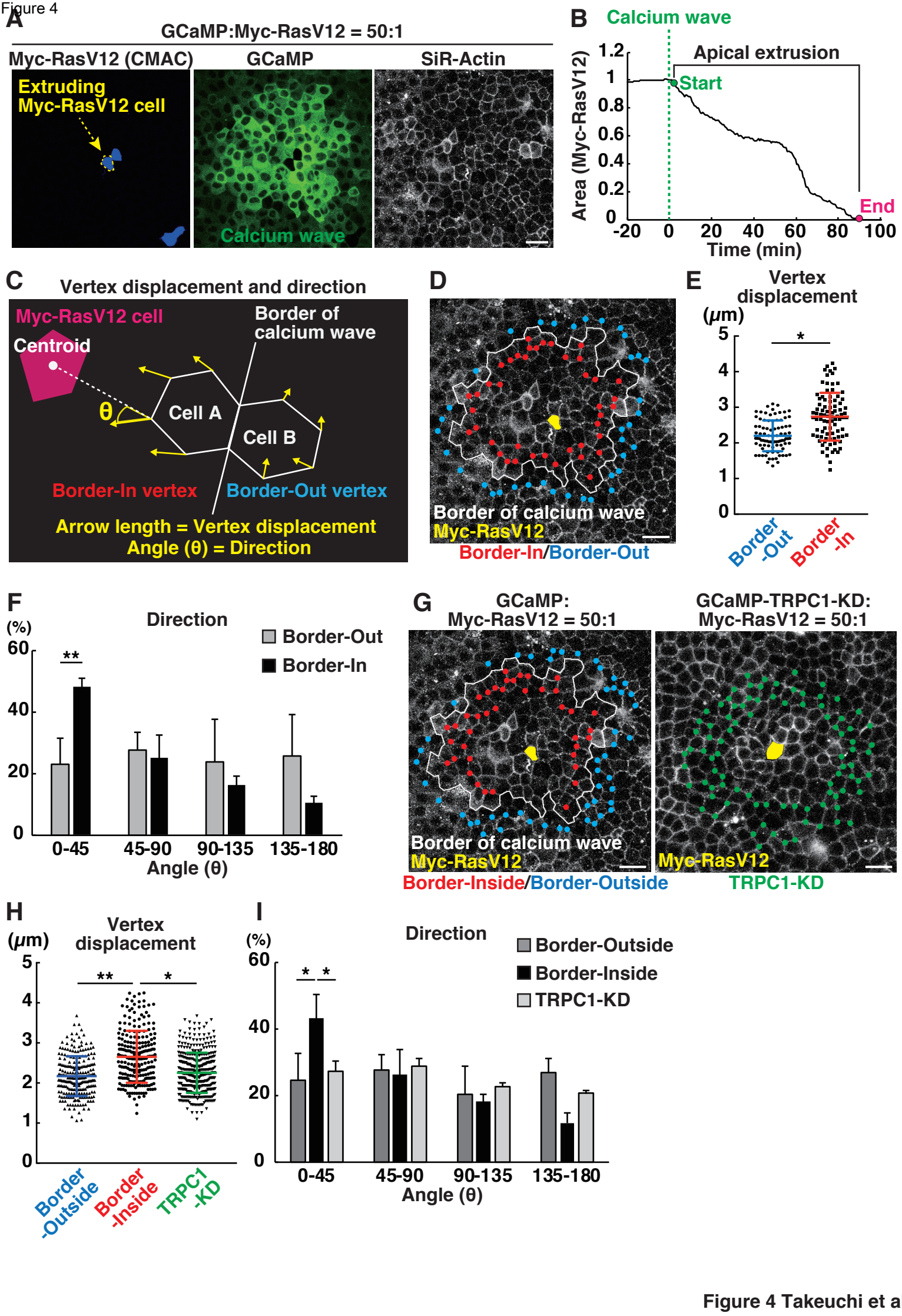

Figure 4 Takeuchi et al.

Figure 5

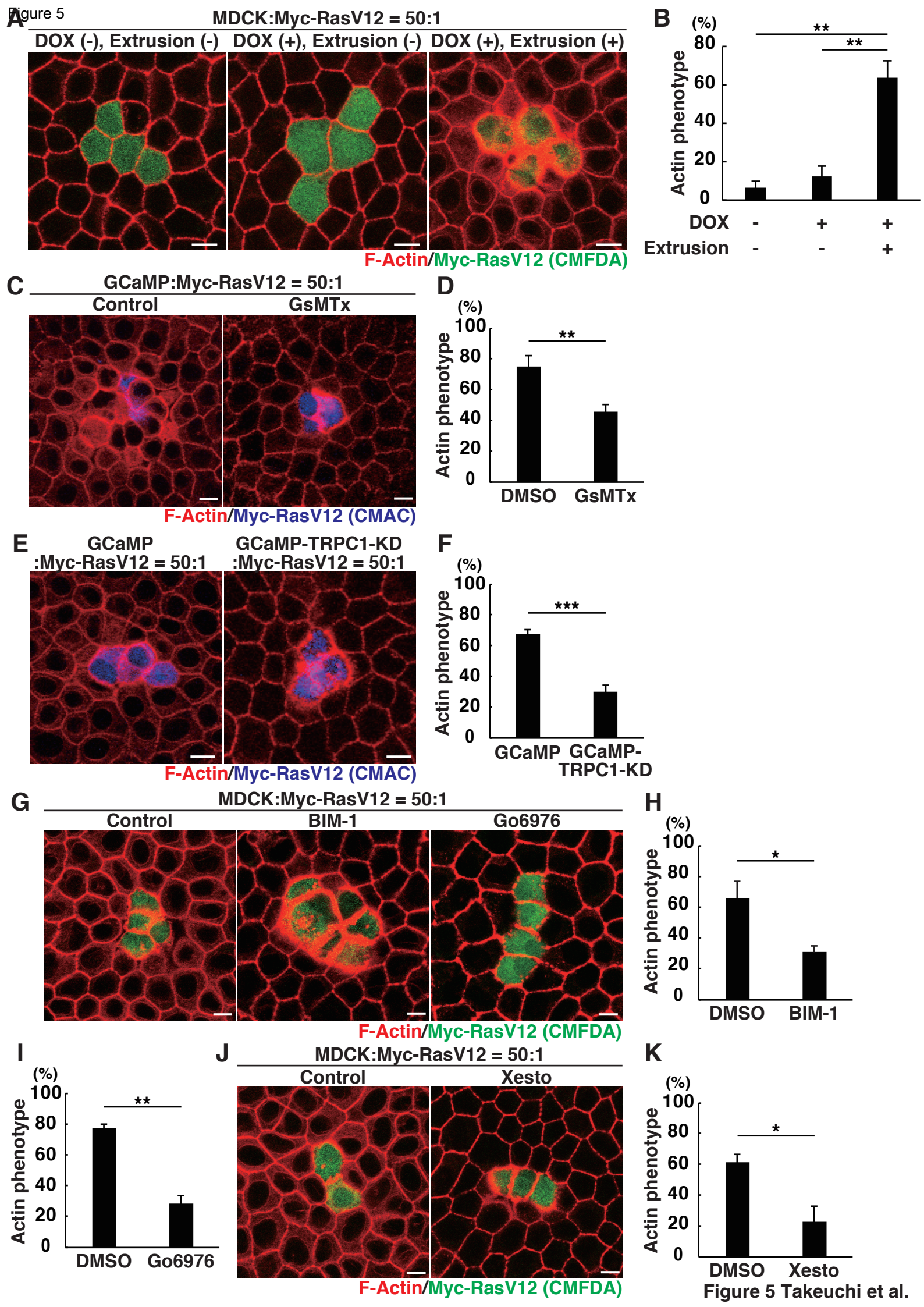

Figure 5 Takeuchi et al.

Figure 6

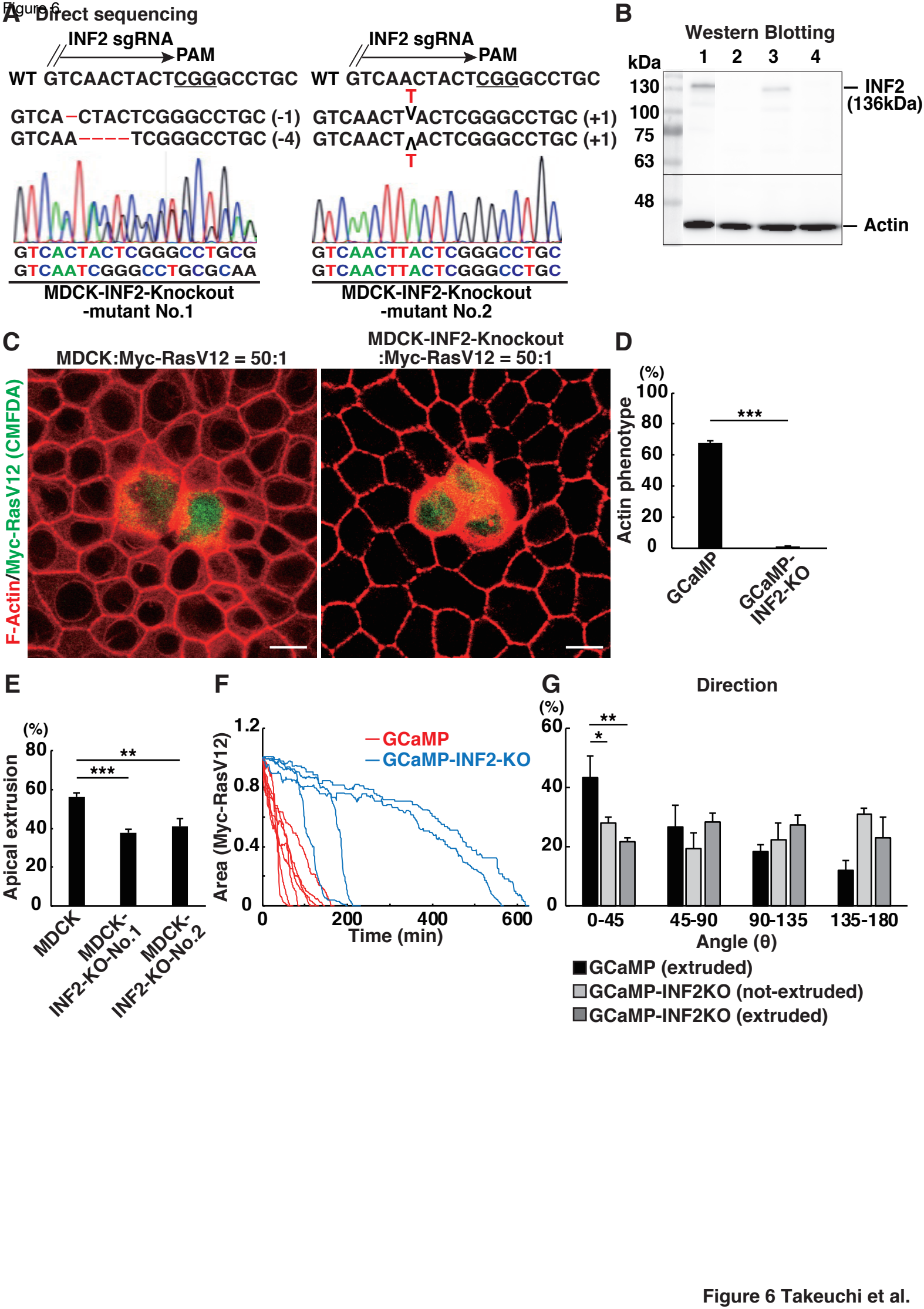

Figure 6 Takeuchi et al.

Figure 7

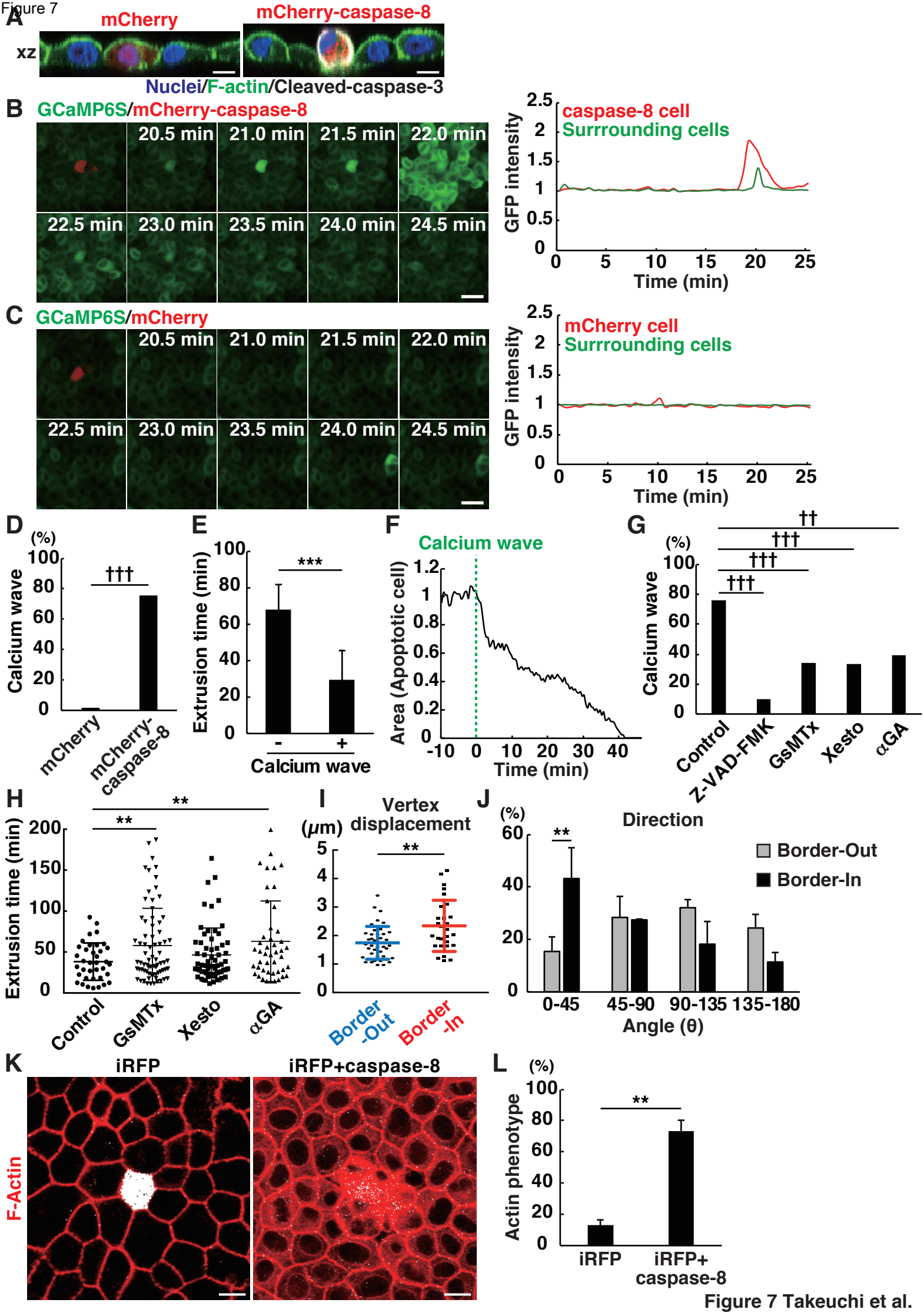

Figure 7 Takeuchi et al.